Progress In Electromagnetics Research, Vol. 129, 143–159, 2012

PROCESSING ONE-STATIONARY BISTATIC SAR DATA USING INVERSE SCALED FOURIER TRANSFORM

J. Wu[1, 2, *], Z. Li[1], Y. Huang[1], Q. Liu[2], and J. Yang[1]

[1]School of Electronic Engineering, University of Electronic Science and Technology of China, No. 2006, Xiyuan Ave., High-tech West Zone, Chengdu 611731, China

[2]Department of Electrical and Computer Engineering, Duke University, Durham, NC 27708, USA

Abstract—In bistatic synthetic aperture radar (SAR) with one stationary station, two-dimensional spatial variance is a major problem which should be handled. In this paper, an Inverse Scaled Fourier Transform (ISFT) imaging algorithm to deal with this problem is proposed. The approach linearizes the two-dimensional spatially-variant point target reference spectrum to derive the reflectivity pattern's spectrum. Based on this spectrum, an ISFT along range direction and a frequency shift along azimuth direction are used to achieve the two-dimensional spatial variance correction. This method is efficient as it only uses phase multiplication and FFTs. Numerical simulations verified the effectiveness of the method.

1. INTRODUCTION

Synthetic Aperture Radar (SAR) uses relative motion between an antenna and its target region to provide high spatial resolution [1–5]. Bistatic SAR has received considerable attentions and research around the world recently [6–9]. Several airborne experiments have been carried out and some spaceborne projects are scheduled as well. One-Stationary bistatic SAR (OS-BSAR) refers to bistatic SAR where azimuth aperture is synthesized by only one moving station, while the other platform is nearly stationary. In this mode, the stationary transmitter or receiver could be mounted on a geostationary satellite,

Received 15 February 2012, Accepted 21 May 2012, Scheduled 17 June 2012

* Corresponding author: Junjie Wu (jw358@duke.edu).

a stratosphere low speed airship, or a ground-based high-altitude platform.

Azimuth spatial variance is rarely an issue in traditional SAR systems, because monostatic SAR and most bistatic SAR with two parallel flying platforms are spatially invariant along azimuth direction. Different from these systems, OS-BSAR is spatially variant in azimuth, because the relative position between transmitter and receiver varies with slow-time [9, 10]. Thus, the targets in a given range bin suffer different Range Cell Migrations (RCM) and Doppler reference functions. Consequently, imaging of OS-BSAR is severely azimuth dependent. Hence, traditional imaging algorithms, like range-Doppler, Chirp-Scaling [11], and Omega-K [12, 13] cannot be used directly because they are all based on the assumption of azimuth invariance.

To improve the OS-BSAR imaging, a Nonlinear Chirp Scaling (NLCS) method has been utilized to equalize the different frequency modulated (FM) rates in the same range bin [10, 14]. However, the method neglects the RCM variation along azimuth direction. This would lead to larger errors when azimuth variance gets large. In [9], the dataset is segmented into several blocks, within which the spatial variance can be neglected. But the approach is only suitable in the specific case where the imaged scene has a small extension in azimuth. In addition, the segmentation reduces the processing efficiency.

Inverse Scaled Fourier Transform (ISFT) is a frequency-domain scaling approach. It uses chirp multiplications and FFTs to correct the scaling in time domain which would be generated if traditional inverse Fourier Transform is used for a linearly scaled signal in frequency domain [15]. It has been used to correct the RCM of monostatic SAR [16]. In this paper, an ISFT imaging algorithm for OS-BSAR is proposed. After we obtain the point target reference spectrum, we express it in terms of a normal spatial coordinate system by two-dimensional Taylor expansion. Then the spectrum of the raw data is expressed as the Fourier transform of the reflectivity pattern. In addition, a range-frequency linearization operation is performed to derive the range-frequency scaling factor. After that, ISFT operation along range frequency and inverse Fourier transform along azimuth frequency are carried out to get the final image.

The rest of this paper is organized as follows: Section 2 gives the signal model of OS-BSAR. Section 3 includes the ISFT algorithm for OS-BSAR. Simulation experiments are given in Section 4. Section 5 concludes this paper.

2. SIGNAL MODEL OF OS-BSAR

In this paper, we always assume the transmitter is stationary. Fig. 1 gives the imaging configuration of OS-BSAR. The coordinate origin O is set to be the scene center. $P(x, y)$ is an arbitrary point target in the imaging area. h_T and h_R are the heights of the transmitter and receiver, respectively. $r_R(x)$ is the receiver slant range of closed approach. R_R and R_T denote the receiver and the transmitter's slant ranges, respectively. The receiver moves above the y axis with a velocity of V.

The slant range of the moving receiver with respect to $P(x, y)$ is:

$$R_R(t; x) = \sqrt{(x - x_R)^2 + (y - Vt - y_R)^2 + h_R^2} \tag{1}$$

where t is slow-time and $t = 0$ when the receiver's wave beam center radiates the scene center O. Differently, the transmitter range is a constant for a certain point target, but changes with target location:

$$R_T(x, y) = \sqrt{(x - x_T)^2 + (y - y_T)^2 + h_T^2} \tag{2}$$

Then the bistatic range history is: $R(t; x, y) = R_T(x, y) + R_R(t; x)$.

The signal reflected from a single point target $P(x, y)$ and after

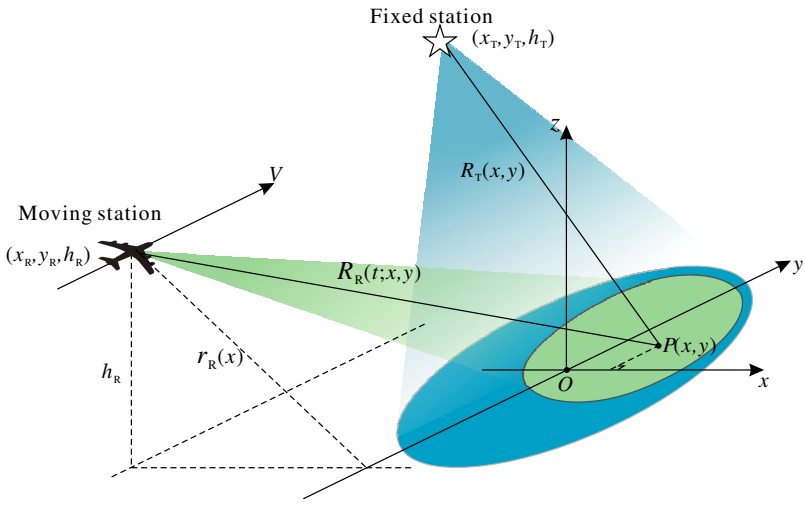

Figure 1. Geometry configuration of OS-BSAR.

demodulation to baseband is (constants are neglected) [10]:

$$\begin{aligned} s(\tau,t;x,y) &= \sigma(x,y)\mathrm{rect}\left[\frac{\tau-\tau_d(t;x,y)}{T_r}\right] w_a\left[\frac{t-t_d(y)}{T_a}\right] \\ &\quad\times\exp\left\{j\pi K_r\left[\tau-\frac{R_T(x,y)+R_R(t;x)}{c}\right]^2\right\} \\ &\quad\times\exp\left\{-j2\pi f_0\frac{R_T(x,y)+R_R(t;x)}{c}\right\} \end{aligned} \tag{3}$$

where $\sigma(x,y)$ is the surface reflectivity pattern, τ is fast time and $\tau_d(t;x,y)$ is the two-way time delay from $P(x,y)$; rect$[\cdot]$ and $w_a[\cdot]$ represent the fast-time and slow-time windows, respectively; $t_d(y) = y/V$ is the slow-time delay; K_r is the frequency modulated rate of the transmitted signal; c is the velocity of light; f_0 is the carrier frequency; T_r and T_a are the window lengthes along fast-time and slow-time directions, respectively.

By using the principle of stationary phase, the signal is transformed into 2D frequency domain [9]:

$$S(f,f_t;x,y) = \sigma(x,y)\mathrm{rect}\left[\frac{f}{B_r}\right] w_a\left[\frac{f_t-f_{dc}}{B_a}\right]\exp\{j\phi(f,f_t;x,y)\} \tag{4}$$

where the phase factor in 2D frequency domain is:

$$\begin{aligned} \phi(f,f_t;x,y) = &-\frac{\pi f^2}{K_r} - 2\pi\frac{(f+f_0)}{c}R_T(x,y) \\ &- 2\pi r_R(x)\sqrt{\left(\frac{f+f_0}{c}\right)^2-\left(\frac{f_t}{V}\right)^2} - 2\pi f_t\frac{y}{V} \end{aligned} \tag{5}$$

where f is range frequency, and f_t represents azimuth frequency. $r_R(x) = \sqrt{(x-x_R)^2+h_R^2}$ is receiver slant range of closed approach. The first phase factor in (5) is range modulation phase. The second one represents the range location influence caused by stationary transmitter. It determines the azimuth variance as well. The third part determines the RCM, azimuth compression and second range compression (SRC). And the last term is the location difference along y axis between $P(x,y)$ and O.

3. ISFT ALGORITHM FOR OS-BSAR

The raw data spectrum can be expressed as an integral [16]:

$$H(f,f_t) = \iint S(f,f_t;x,y)dxdy \tag{6}$$

The aim of focusing is to invert this integral and deduce $\sigma(x, y)$, the bistatic scattering coefficient for the whole scene. However, it is not easy to solve this integral directly, because in OS-BSAR $\phi(f, f_t; x, y)$ has complicated nonlinear relationships with x and y.

3.1. Spatial Domain Linearization

Here we choose r_R (r_R is short for $r_R(x)$) and y as final image coordinates, because they are normal to each other and the nonlinear part of (5) is linear with r_R.

Firstly R_T is expressed as a function of r_R and y:

$$R_T(r_R, y) = \sqrt{\left(\sqrt{r_R^2 - h_R^2} + x_R - x_T\right)^2 + (y - y_T)^2 + h_T^2} \tag{7}$$

Then it is linearized in terms of $(r = r_R - r_{R0}, y)$ at $(r_R = r_{R0}, y = 0)$, where r_{R0} is the receiver slant range of closed approach of the scene center:

$$R_T(r_R, y) \approx R_{T0} + ar + by \tag{8}$$

where $R_{T0} = R_T(r_{R0}, 0)$, $a = \partial R_T(r_R, y)/\partial r_R|_{r_R = r_{R0}, y=0}$, $b = \partial R_T(r_R, y)/\partial y|_{r_R = r_{R0}, y=0}$.

By substituting (8) into (5), $\phi(f, f_t; x, y)$ can be decomposed into space-invariant component, range-variant and azimuth-variant terms:

$$\phi(f, f_t; x, y) \approx \phi_0(f, f_t) + \phi_{rg}(f, f_t; r) + \phi_{az}(f, f_t; y) \tag{9}$$

where $\phi_0(f, f_t) = \phi(f, f_t; r_{R0}, 0)$, $\phi_{rg}(f, f_t; r) = -2\pi r\xi(f, f_t)$, $\xi(f, f_t) = a(f + f_0)/c + \sqrt{(f + f_0)^2/c^2 - (f_t/V)^2}$, $\phi_{az}(f, f_t; y) = -2\pi y\eta(f, f_t)$, $\eta(f, f_t) = b(f + f_0)/c + f_t/V$. $\phi_0(f, f_t)$ is spatially invariant in the whole scene. It includes the range compression, bulk RCM correction, bulk azimuth compression and bulk SRC. So, it can be compensated by a phase multiplication. $\phi_{rg}(f, f_t; r)$ and $\phi_{az}(f, f_t; y)$ are the range-variant and azimuth-variant components, respectively.

Till now, the raw data spectrum of the scene can be written as:

$$\begin{aligned} H(f, f_t) &= \text{rect}\left[\frac{f}{B_r}\right] w_a\left[\frac{f_t - f_{dc}(x, y)}{B_a}\right] \exp[j\phi_0(f, f_t)] \\ &\quad \iint \sigma(r, y) \exp\left[-j2\pi y\eta(f, f_t)\right] \times \exp[-j2\pi r\xi(f, f_t)]\, dr dy \\ &= H_0(f, f_t) \times \Gamma[\xi(f, f_t), \eta(f, f_t)] \end{aligned} \tag{10}$$

where

$$H_0(f, f_t) = \text{rect}\left[\frac{f}{B_r}\right] w_a\left[\frac{f_t - f_{dc}(x, y)}{B_a}\right] \exp[j\phi_0(f, f_t)] \tag{11}$$

$\Gamma[\xi(f, f_t), \eta(f, f_t)]$ is the 2D Fourier transform of $\sigma(r, y)$. If we perform 2D inverse FFT to $\Gamma[\xi(f, f_t), \eta(f, f_t)]$, we can get the 2D scattering pattern of the imaging scene, that is the final microwave image. However, as we can find that $\xi(f, f_t)$ is nonlinear with f, the 2D inverse FFT is not easy to be carried out directly.

3.2. Frequency Domain Linearization

In (10), $\eta(f, f_t)$ is linear with f_t and is an azimuth frequency shift which varies with range frequency. According to the frequency shift property of Fourier transform, this frequency shift can be corrected via phase factor multiplication in the domain of azimuth time and range frequency. The phase factor for this correction is:

$$\phi_{azs}(f, t) = -2\pi \frac{b(f + f_0)V}{c} t \tag{12}$$

In fact, this phase can also be viewed as a range frequency domain phase factor at each azimuth time t. The result of this phase multiplication is a location shift along bistatic range axis. The shift is $\Delta\tau(t) = bVt/c$.

In OS-BSAR, targets with the same r_R fall in different range gates. The difference between the range gates of $P(r_R, y)$ and $P(r_R, 0)$ is:

$$R_T(r_R, y) - R_T(r_R, 0) \approx by = \Delta\tau(t)c \tag{13}$$

Hence, the effect of $\exp\{-j\phi_{azs}(f, t)\}$ multiplication is to align the different range locations of the targets which have the same r_R.

Differently, $\xi(f, f_t)$ is nonlinearly dependent on f. To use ISFT, we further expand $\xi(f, f_t)$ in the first-order Taylor series in terms of f:

$$\xi(f, f_t) \approx I_{rg}^{RCM}(f_t) f + I_{rg}^{C} + I_{rg}^{AZC}(f_t) \tag{14}$$

where $I_{rg}^{RCM}(f_t) = a/c + 1/[cD(f_t)]$, $I_{rg}^{C} = af_0/c$, $I_{rg}^{AZC}(f_t) = f_0 D(f_t)/c$ and $D(f_t) = \sqrt{1 - c^2 f_t^2/(V^2 f_0^2)}$.

Some further comments concerning (14) are given as follows:

- $I_{rg}^{RCM}(f_t) f$ is a linear term of f. It can be rewritten as:

$$I_{rg}^{RCM}(f_t) f \approx \frac{1}{c}\left[\left(a + \frac{1}{D(f_{dc})}\right) f + \left(\frac{1}{D(f_t)} - \frac{1}{D(f_{dc})}\right) f\right] \tag{15}$$

  where f_{dc} is the Doppler centroid. $[1/D(f_t) - 1/D(f_{dc})]\, f$ is a scaling of range frequency. Its scaling factor varies with azimuth frequency and represents the residual RCMC. This is the same with monostatic SAR [16, 17].

  The constant scaling term $[a + 1/D(f_{dc})]f$ involves a stretching of the range frequency axis by a constant factor $a + 1/D(f_{dc})$.

This stretching in range frequency will lead to a linear scaling of fast-time axis.

After the frequency shift correction in (12), the difference between the range gates of targets which have the same r_R and r_{R0} is:

$$\begin{aligned}\Delta R_{bi}(r_R; r_{R0}) &= R_T(r_R, 0) - R_T(r_{R0}, 0) + \frac{r_R}{\cos\theta(r_R)} - \frac{r_{R0}}{\cos\theta(r_{R0})} \\ &\approx ar + \frac{r}{\cos\theta(r_{R0})} \end{aligned} \tag{16}$$

And we have $D(f_{dc}) = \sqrt{1 - c^2 f_{dc}^2/(V^2 f_0^2)} = \cos\theta(r_{R0})$, so

$$\Delta R_{bi}(r_R; r_{R0}) = r\left(a + \frac{1}{D(f_{dc})}\right) \tag{17}$$

Therefore, the effect of this constant scaling term is to scale the range axis which was the bistatic range of R_{bi} to the receiver slant range of closed approach of r_R.

According to the frequency scaling method using chirp signals [15, 16], the scaling of $I_{rg}^{RCM}(f_t)$ can be corrected by ISFT.

- $I_{rg}^{AZC}(f_t) = f_0 D(f_t)/c$ is a constant shift of range frequency. It represents the residual azimuth modulation.

3.3. Processing Procedures

This subsection gives the processing steps of the algorithm:

(1) Transform raw data into two-dimensional frequency domain.

(2) Reference function multiplication (RFM) by the conjugate of $H_0(f, f_t)$ in (11). It can remove the spatial-invariant phase modulation.

(3) Azimuth inverse FFT. It is formulated as:

$$\begin{aligned} H_1(f, y) &= \int \Gamma[\xi(f, f_t), \eta(f, f_t)] \exp(j2\pi f_t t) df_t \\ &= \Gamma[\xi(f, f_t), y] \times \exp\{j\phi_{azs}(f, y/V)\} \end{aligned} \tag{18}$$

(4) Azimuth-variant term correction and azimuth FFT. The compensation phase factor is $\exp\{-j\phi_{azs}(f, y/V)\}$. After azimuth FFT, we get $\Gamma[\xi(f, f_t), f_t/V]$.

(5) Range frequency scaling. This step employs ISFT to achieve the frequency scaling. It can also be finished by Chirp-Scaling.

$$\begin{aligned} H_2(r, f_t) &= \int \Gamma[\xi(f, f_t), f_t/V] \exp\{j2\pi I_{rg}^{RCM}(f_t) ft\} df \\ &= \sigma(r, f_t/V) \times \exp\left[-j2\pi \left(I_{rg}^{AZC}(f_t) + I_{rg}^{C}\right) r\right] \end{aligned} \tag{19}$$

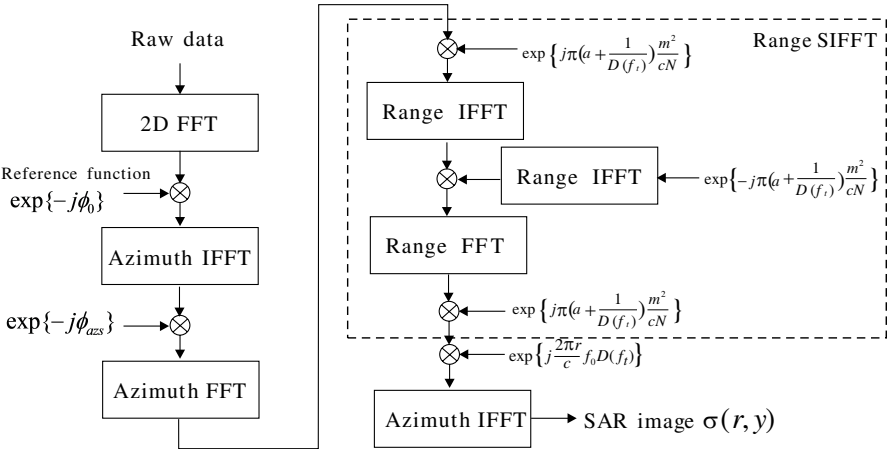

Figure 2. Block diagram of the ISFT algorithm for OS-BSAR.

(6) Residual azimuth compression. In the domain of $(r, f_t/V)$, the residual azimuth compression can be performed by multiplying $\exp\left[j2\pi I_{rg}^{AZC}(f_t)r\right]$. After that, by using the traditional inverse Fourier transform, the final image can be generated.

Figure 2 shows the flowchart of the ISFT algorithm for OS-BSAR in this paper. This method just needs phase multiplication and FFT operations. So the computing efficiency can be guaranteed.

The above algorithm uses 4 times of FFT and IFFT on azimuth direction, and 4 times of FFT and IFFT on range direction. The residual operation is the 5 times of 2D phase factor multiplication. Suppose the range sample number is N_r while the azimuth sample number is N_a. The total number of real floating-point operations would now be:

$$20N_aN_r\log_2(N_a) + 20N_aN_r\log_2(N_r) + 30N_aN_r \tag{20}$$

So the computational complexity is of order $O(N^2\log_2 N)$, where N is one dimensional size of the data.

3.4. Limitations and Error Analysis

The proposed ISFT algorithm for OS-BSAR is based on the linearization of the 2D spectrum phase factor. When the stationary transmitter's beam direction is nearly vertical to the moving receiver's flight path, if we choose the scene center to be the reference point, b in (8) will nearly be zero. The target displacement along range direction which is caused by the stationary transmitter will be quadratic with y.

So the phase factor in (12) cannot achieve the location correction. In addition, when the receiver works with the forward-looking mode [18], a in (8) will be infinite. So if the algorithm is applied in the two cases discussed above, the performance will not be as good as that in other one-stationary bistatic cases.

Here based on the residual error analysis, we will give the limitations of the proposed ISFT algorithm. In OS-BSAR, the azimuth spatial variance would lead to the different azimuth frequency modulated rates and RCMs along azimuth direction. Because the quadratic terms in the Taylor series expansion is the most dominant component, the truncated error term can be approximately determined by the quadratic term:

$$\Delta R_T(r_R, y) = a' r^2 + b' y^2 \tag{21}$$

where a' and b' are the second order Taylor coefficients of $R_T(r_R, y)$ with respect to r and y, respectively. In the same range gate, the residual error of receiver's central slant range equals to $\Delta R_T(r_R, y)$:

$$\frac{\Delta r_R(r_R, y)}{\cos(\theta)} = \Delta R_T(r_R, y) \tag{22}$$

where $\Delta r_R(r_R, y)$ is the residual error of receiver's closed range, θ is the squint angle of receiver.

To neglect the influence of linearization, the quadratic phase error (QPE) resulted from the linearization should be less than $\pi/4$. At the same time, the error of RCM should be less than one slant range resolution cell.

The limitation of QPE can be written as:

$$\text{QPE} = \pi T^2 \left| (-f_R / r_{R0}) \Delta r_R \right| / 4 < \frac{\pi}{4} \tag{23}$$

where T is the synthetic aperture time and f_R the azimuth modulated rate of the reference point.

So we have

$$|\Delta r_R| < \frac{\lambda r_{R0}^2}{V^2 T^2 \cos(\theta)^3} = \frac{D_{\text{aper}}^2}{\lambda} \cos(\theta) \tag{24}$$

where D_{aper} is the receiver's antenna aperture length in azimuth direction.

The limitation of RCM can be written as:

$$\Delta r_R \left(\frac{1}{D(f_t)} - 1 \right) < \delta r \tag{25}$$

where δr is the slant range resolution. In OS-BSAR, $\delta r = c/B_r$. Then we can get the receiver range difference which is computed by the

residual RCM criterion:

$$\Delta r_R = \delta r \min\left(\frac{D(f_t)}{1 - D(f_t)}\right) \tag{26}$$

So the limitation condition of the algorithm in this paper can be written as:

$$\max\{a' r^2 + b' y^2\} < \min\left\{\frac{D_{\text{aper}}^2}{\lambda}, \frac{\delta r}{\cos(\theta)} \min\left(\frac{D(f_t)}{1 - D(f_t)}\right)\right\} \tag{27}$$

For side-looking or squint looking OS-BSAR, the linearization of R_T with r generally is satisfied. The applicability of this algorithm for OS-BSAR mainly depends on b'. As for forward-looking OS-BSAR, a is infinite. The linear relationship between R_T and r does not establish at all. So, the method in this paper can not be applied in forward-looking mode of OS-BSAR.

As for the linearization of the frequency, this approximation neglects the spatial variance of the second range compression. This is the limitation of the algorithms based on ISFT, Chirp-Scaling and range-Doppler.

4. NUMERICAL SIMULATION

4.1. Imaging Performance Simulation

To verify the effectiveness of the proposed algorithm, we carry out numerical simulations of two geometry cases in this section. In case I, we simulated the focusing performance of the proposed algorithm for the mode in which the transmitter is on a near-space airship with the coordinates of $(-50,\ -10,\ 36)$ km. To present the generality of the algorithm, the receiver works in squint mode. Its coordinates at $t = 0$ are $(-12,\ -10,\ 10)$ km. The carrier frequency is 9.6 GHz and

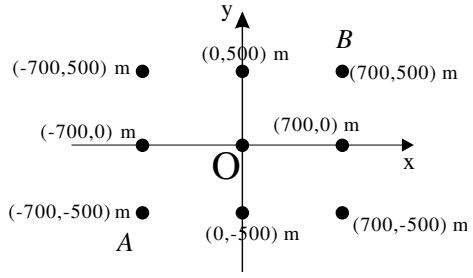

Figure 3. Target area used in the simulation.

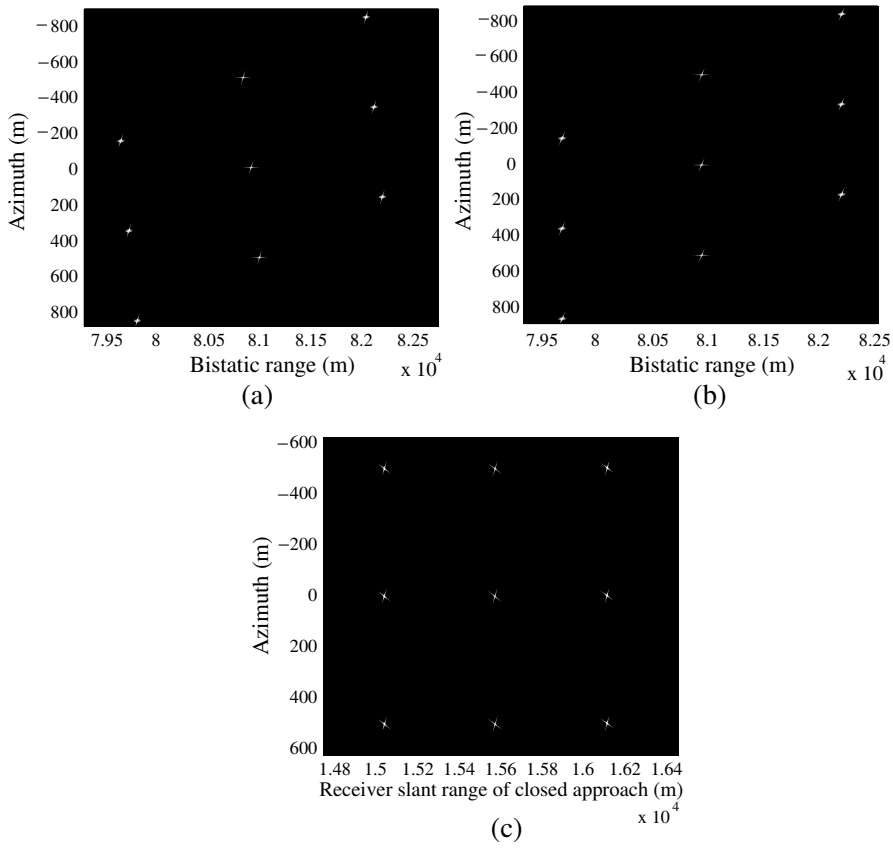

Figure 4. Imaging results of Case I. (a) Time domain result after RFM. (b) Time domain result after azimuth frequency shift. (c) Final imaging result.

the bandwidth of transmitted signal is 70 MHz. PRF is 400 Hz and the velocity of the moving platform is 200 m/s. In order to highlight the capacity of processing and the 2D spatially variant feature, in the scene we set 9 point targets, which are located on the vertices of a 3×3 matrix as shown in Fig. 3. The imaging results in this case is shown in Fig. 4. Figs. 4(a)–4(c) give the time domain results after RFM, azimuth frequency shift and azimuth residual compression, respectively.

In case II, the transmitter is on a geostationary satellite with the coordinates of $(-200,\ -200,\ 36000)$ km, while the receiver works in side-looking mode with the coordinates of $(-12, 0, 10)$ km. The other parameters are the same with those in case I. The imaging results are

shown in Fig. 5.

In addition, the performance of this algorithm is also compared with that of back-projection algorithm. To quantify the precision of the presented processing method, the impulse-response width (IRW),

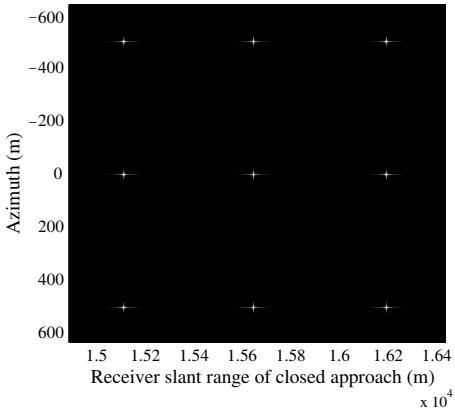

Figure 5. Final imaging result of case II.

Table 1. Imaging quality parameters for Case I.

		Range		
		IRW (m)	PSLR(dB)	ISLR(dB)
ISFT	Target A	3.84	−12.72	−10.10
	Target O	3.80	−13.32	−10.17
	Target B	3.86	−12.80	−10.12
BP	Target A	3.80	−13.30	−10.15
	Target O	3.80	−13.32	−10.19
	Target B	3.82	−13.31	−10.18
		Azimuth		
		IRW (m)	PSLR(dB)	ISLR(dB)
ISFT	Target A	1.52	−12.98	−10.13
	Target O	1.53	−13.33	−10.22
	Target B	1.58	−13.10	−10.15
BP	Target A	1.51	−13.30	−10.25
	Target O	1.52	−13.34	−10.19
	Target B	1.56	−13.32	−10.20

Table 2. Imaging quality parameters for Case II.

		Range		
		IRW (m)	PSLR(dB)	ISLR(dB)
ISFT	Target A	3.80	−13.27	−10.19
	Target O	3.80	−13.27	−10.17
	Target B	3.81	−13.28	−10.18
BP	Target A	3.80	−13.27	−10.19
	Target O	3.80	−13.27	−10.18
	Target B	3.80	−13.28	−10.18
		Azimuth		
		IRW (m)	PSLR(dB)	ISLR(dB)
ISFT	Target A	1.04	−13.29	−10.17
	Target O	1.08	−13.32	−10.18
	Target B	1.12	−13.02	−10.05
BP	Target A	1.04	−13.29	−10.16
	Target O	1.08	−13.32	−10.18
	Target B	1.12	−13.28	−10.17

peak sidelobe ratio (PSLR), and integrated sidelobe ratio (ISLR) are used as quality criteria. These quality parameters are shown in Table 1 and Table 2.

To facilitate the quality analysis in the simulation, we do not consider the influence of the bistatic geometry on resolution measurement. Otherwise, some additional projection computation should be made to get the resolution results on the ground plane. That is, the theoretical range resolution is $0.886(c/B_r) = 3.80\,\text{m}$, where B_r is the transmitted signal bandwidth. The azimuth resolution is $0.886(c/B_d)$ where B_d means the Doppler bandwidth. In our simulations, we assume the synthetic aperture time is a constant. So the theoretical resolution along azimuth direction is a function of target location. In case I, the azimuth resolutions of A, O and B are 1.50 m, 1.52 m and 1.55 m, respectively. As for the second case, the theoretical azimuth resolutions of A, O and B are 1.04 m, 1.08 m and 1.12 m, respectively. The Doppler bandwidth of these three targets are 158.6 Hz, 163.9 Hz and 158.4 Hz, respectively.

From these two tables, we can find that, the focusing performance along range direction of the proposed method is almost the same with that of BP method and the theoretical result. As for the azimuth

direction, only the PSLR and ISLR have little derivations from the BP results. The measured azimuth resolution has a maximum broadening of 2% and range resolution has a broadening of 1.6% in comparison with the theoretical values.

4.2. Limitation Simulation

Because the frequency domain linearization used in (14) is accordant with the algorithms based on ISFT [16], here we just carry on simulations to discuss the spatial linearization made in (8).

Firstly, the transmitter's beam direction is vertical to the flight path of the receiver. It is on a ground-based platform with the

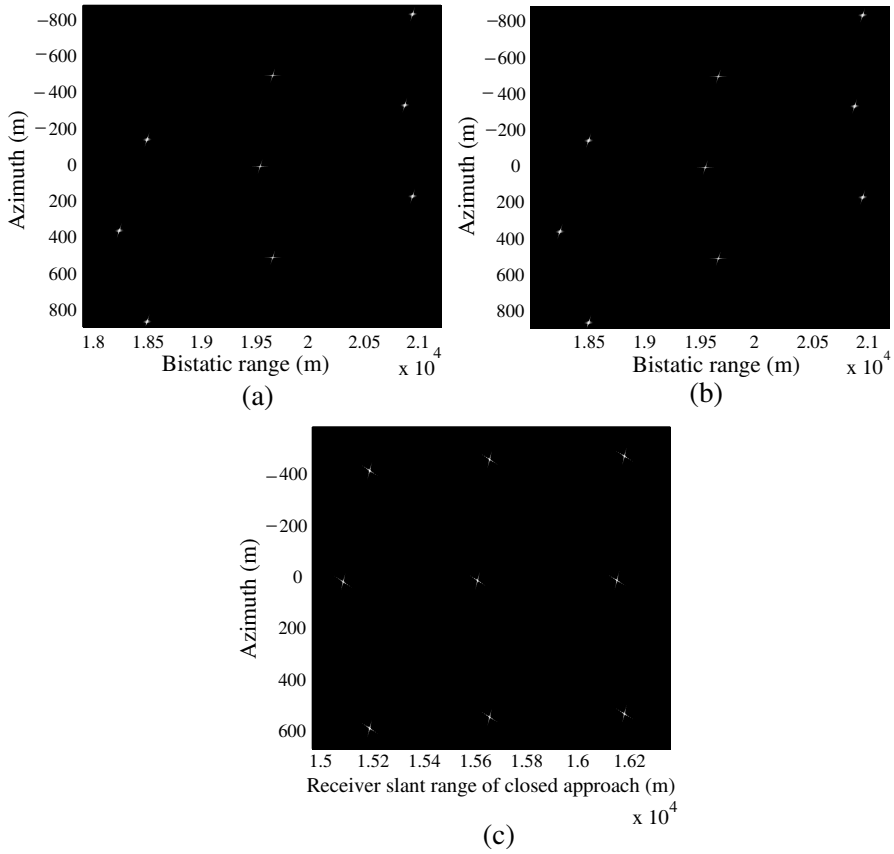

Figure 6. Imaging results of Case III. (a) Time domain result after RFM. (b) Time domain result after azimuth frequency shift. (c) Final imaging result.

coordinates of $(-1.5,\ -0,\ 0.36)$ km. The receiver works in squint mode as the same as in case I. In this mode, b in (8) is zero. So the phase factor in (12) cannot achieve the location correction. $a' = 3.58 * 10^{-6}\,\mathrm{m}^{-1}$, $b' = 4.9 * 10^{-4}\,\mathrm{m}^{-1}$, $a'r^2 = 1.8$ m, $b'y^2 = 123$ m. The right part of (26) is 27 m, which is much less than $b'y^2$. Then the azimuth spatial variance will still exist. The imaging results for this mode are shown in Fig. 6(a)–Fig. 6(c). Because of the severe azimuth spatial variance and the failing of correction effect of (8), the result shows displacement and a little defocus.

Secondly, the receiver works in forward-looking mode. In this mode, the transmitter's coordinates are $(-12000,\ -5000,\ 20000)$ m

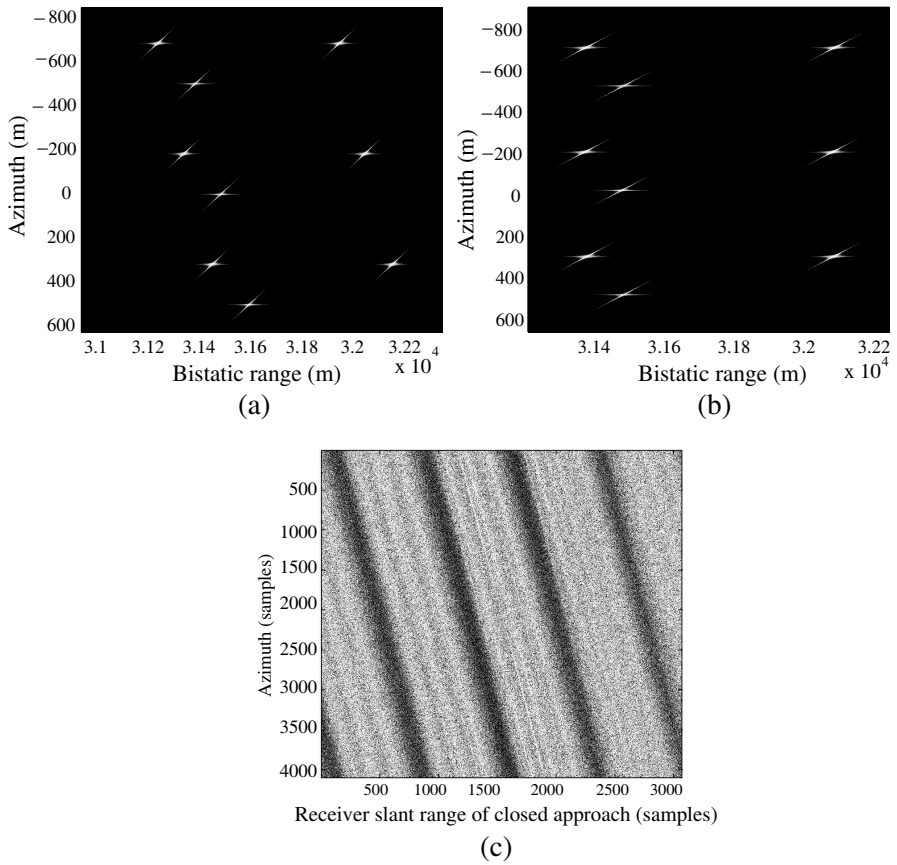

Figure 7. Imaging results of Case IV. (a) Time domain result after RFM. (b) Time domain result after azimuth frequency shift. (c) Final result.

while the receiver's coordinates are (0, −7000, 3000) m. As stated in Section 3, a in (8) will be infinite. The imaging results for this mode are shown in Fig. 7. Because of the ineffectiveness of this method for forward-looking mode, it even can not get a reasonable image at all.

5. CONCLUSION

An ISFT algorithm for dealing with the two-dimensional spatial variance in One-Stationary Bistatic SAR data was presented in this paper. In this paper, the spectrum of the raw data is linearized in space and frequency domain. Based on the linearization result, azimuth correction phase factor and range ISFT factor were deduced. Simulation results show that the proposed algorithm has an effective ability to focus the data with one-stationary bistatic configuration.

ACKNOWLEDGMENT

This work is supported by the National High-tech Research and Development Program (863 Program) of China (No. 2009AA12Z106), and the Fundamental Research Funds for the Central Universities (No. A03006023901007).

REFERENCES

1. Lim, S., J. Han, S. Kim, and N. Myung, "Azimuth beam pattern synthesis for airborne SAR system optimization," *Progress In Electromagnetics Research*, Vol. 106, 295–309, 2010.
2. Wei, S., X. Zhang, J. Shi, and G. Xiang, "Sparse reconstruction for SAR imaging based on compressed sensing," *Progress In Electromagnetics Research*, Vol. 109, 63–81, 2010.
3. Xu, W., P. Huang, and Y. Deng, "Multi-channel SPCMB-TOPS SAR for high-resolution wide-swath imaging," *Progress In Electromagnetics Research*, Vol. 116, 533–551, 2011.
4. Wei, S., X. Zhang, and J. Shi, "Linear array SAR imaging via compressed sensing," *Progress In Electromagnetics Research*, Vol. 117, 299–319, 2011.
5. Liu, Q., W. Hong, W. Tan, et al, "An improved polar format algorithm with performance analysis for geosynchronous circular SAR 2D imaging," *Progress In Electromagnetics Research*, Vol. 119, 155–170, 2011.

6. Wu, J., J. Yang, Y. Huang, Z. Liu, and H. Yang, "A new look at the point target reference spectrum for bistatic SAR," *Progress In Electromagnetics Research*, Vol. 119, 363–379, 2011.
7. Sun, J., S. Mao, G. Wang, and W. Hong, "Polar format algorithm for spotlight bistatic SAR with arbitrary geometry configuration," *Progress In Electromagnetics Research*, Vol. 103, 323–338, 2010.
8. Dai, C. and X. Zhang, "Omega-k algorithm for bistatic SAR with arbitrary geometry configuration," *Journal of Electromagnetic Waves and Applications*, Vol. 25, Nos. 11–12, 1564–1576, 2011.
9. Wang, R., O. Loffeld, Y. Neo, H. Nies, I. Walterscheid, T. Espeter, J. Klare, and J. Ender, "Focusing bistatic SAR data in airborne/stationary configuration," *IEEE Trans. Geosci. Remote Sens.*, Vol. 48, No. 1, 452–465, 2010.
10. Wong, F. W. and T. S. Yeo, "New applications of nonlinear chirp scaling in SAR data processing," *IEEE Trans. Geosci. Remote Sens.*, Vol. 39, No. 5, 946–953, 2001.
11. Wang, X., D. Zhu, and Z. Zhu, "An implementation of bistatic PFA using chirp scaling," *Journal of Electromagnetic Waves and Applications*, Vol. 5, No. 6, 745–753, 2010.
12. Guo, D., H. Xu, and J. Li, "Extended wavenumber domain algorithm for highly squinted sliding spotlight SAR data processing," *Progress In Electromagnetics Research*, Vol. 114, 17–32, 2011.
13. Mao, X., D. Zhu, L. Ding, and Z. Zhu, "Comparative study of RMA and PFA on their responses to moving target," *Progress In Electromagnetics Research*, Vol. 110, 103–124, 2010.
14. Qiu, X., D. Hu, and C. Ding, "An improved NLCS algorithm with capability analysis for one-stationary BiSAR," *IEEE Trans. Geosci. Remote Sens.*, Vol. 46, No. 10, Part 2, 3179–3186, 2008.
15. Papoulis, A., *Systems and Transforms with Applications in Optics*, McGraw-Hill, Now York, 1968.
16. Franceschetti, G. and R. Lanari, *Synthetic Aperture Radar Processing*, CRC, 1999.
17. Cumming, I. G. and F. H. Wong, *Digital Processing of Synthetic Aperture Radar Data: Algorithms and Implementation*, Artech House, 2005.
18. Qiu, X., D. Hu, and C. Ding, "Some reflections on bistatic SAR of forward-looking configuration," *IEEE Geosci. Remote Sens. Letters*, Vol. 5, No. 4, 735–739, 2008.